www.MaterialsViews.com

**ADVANCED
ELECTRONIC
MATERIALS**

www.advelectronicmat.de

COMMUNICATION

Ligand-Induced Control of Photoconductive Gain and Doping in a Hybrid Graphene–Quantum Dot Transistor

Lyudmila Turyanska,* Oleg Makarovsky, Simon A. Svatek, Peter H. Beton, Christopher J. Mellor, Amalia Patanè, Laurence Eaves, Neil R. Thomas, Michael W. Fay, Alexander J. Marsden, and Neil R. Wilson

Recent advances in graphene-based electronics range from the discovery of fundamental physical phenomena to the development of new high-performance photosensitive devices.[1–5] These applications exploit not only the unique electronic properties of graphene but also additional functionalities that can be achieved by capping the graphene layer with another material or nanostructure, e.g., atomically thin films,[6,7] carbon nanotubes[8] or inorganic nanoparticles.[8–10] Colloidal semiconductor quantum dots (QDs) are of particular interest as their optical properties can be fine-tuned by varying their size and/or composition.[11] In addition, colloidal synthesis enables QDs to be functionalized by doping[12] and/or surface encapsulation.[13] Recently, a photoresponsivity of 10^7 A W^{-1} was achieved by depositing QDs on graphene and explained in terms of trapping of photoexcited carriers on the QDs and charge transfer between them and the graphene layer.[9,10] This mechanism should be strongly dependent on the interface between the QDs and graphene. Furthermore, the ligands that encapsulate the QDs may provide a means of modifying the transfer of electronic charges and enhancing the electronic properties of the graphene layer.

Here, we investigate the properties of single layer graphene (SLG) functionalized with an overlayer of near-infrared PbS colloidal quantum dots capped with thioglycerol/dithioglycerol or polyethylene glycol (PEG500 and PEG2000). We demonstrate that the polarity of the conductivity and the carrier concentration can be modified, and photoresponsivity of SLG can be significantly enhanced by the choice of ligands. By reducing the length of capping ligands, hence the thickness of the dielectric barrier between the QDs and the SLG, and by preserving the integrity of the ligand layer, we achieve the efficient transfer of photogenerated carriers from the QDs to the graphene before recombining, resulting in enhanced photoresponsivities of up to ≈10^9 A W^{-1}.

Single layer graphene grown by low-pressure chemical vapor deposition (LP-CVD)[14,15] was processed into a planar transistor and deposited onto a SiO$_2$/n-Si substrate with oxide layer thickness $t = 300$ nm, as shown schematically in **Figure 1**a (see also the Supporting Information, Figure S1). The length, L, and width, w, of the graphene channel are 6 and 10 μm, respectively. The n-Si layer serves as a gate electrode. Colloidal quantum dots with an average PbS core diameter of $d_{QD} = 4.5$nm (Figure 1b) were stabilized using the following capping ligands of different length, l, which determines the effective separation between the PbS nanocrystals and graphene: polyethylene glycol H—(O—CH$_2$—CH$_2$)$_n$—OH with $n = 2000$ for QD$_{p2000}$ and $n = 500$ for QD$_{p500}$[16]and corresponding length of $l \approx 10$ nm and $l \approx 5$ nm, respectively;[17] a mixture of thioglycerol (TGL) and 2,3-dimercapto-1-propanol (DTG), $l \approx 0.5$ nm for QD$_{TGL}$,[18] see **Table 1**. We note that the ligand size is estimated for extended molecules and does not include any effects that could arise from compression of the ligand layer upon drying under vacuum. The interparticle distances observed on TEM images are comparable with the theoretical estimate of the ligand length (see the Supporting Information, Figure S2). The QDs were drop-cast from aqueous solution (5 mg mL^{-1}) to produce continuous thick (>100 nm) coverage of the graphene layer, followed by drying for 12 h in vacuum at room temperature. The size of the QDs and their room temperature photoluminescence spectra (with a peak at photon energy ≈1.1eV) are similar in all three structures, i.e., they are not affected by the ligand. All measured devices demonstrate stable and reproducible behavior during the measurement period of at least 14 days. All samples were stored in dry nitrogen cabinet and all electrical measurements were performed at room temperature $T = 300$ K in vacuum (≈10^{-6} mbar). The $I(V_g)$ characteristics were measured using slow sweeping rate, r, of the gate voltage, i.e., $r \leq 0.02$ V s^{-1}.

The pristine monolayer graphene devices show a linear dependence of current, I, on bias voltage, V_s, and a minimum conductance at a gate voltage, $V_g^{min} \approx +30$V corresponding to p-type doping with hole concentration, $p \approx 2 \times 10^{12}$ cm^{-2}, typical of CVD graphene[19,20] (Supporting Information, Figure S1). The deposition of the PbS QDs onto the SLG leads to significant

Dr. L. Turyanska, Dr. O. Makarovsky, S. A. Svatek,
Prof. P. H. Beton, Prof. C. J. Mellor,
Prof. A. Patanè, Prof. L. Eaves
School of Physics and Astronomy
The University of Nottingham
Nottingham NG7 2RD, UK
E-mail: Lyudmila.Turyanska@nottingham.ac.uk
Prof. N. R. Thomas
Centre for Biomolecular Sciences
School of Chemistry
The University of Nottingham
Nottingham NG7 2RD, UK
Dr. M. W. Fay
Nottingham Nanotechnology and Nanoscience Centre
Nottingham NG7 2RD, UK
A. J. Marsden, Dr. N. R. Wilson
Department of Physics
University of Warwick
Coventry CV4 7AL, UK

The copyright line of this paper was amended 17 June 2015.
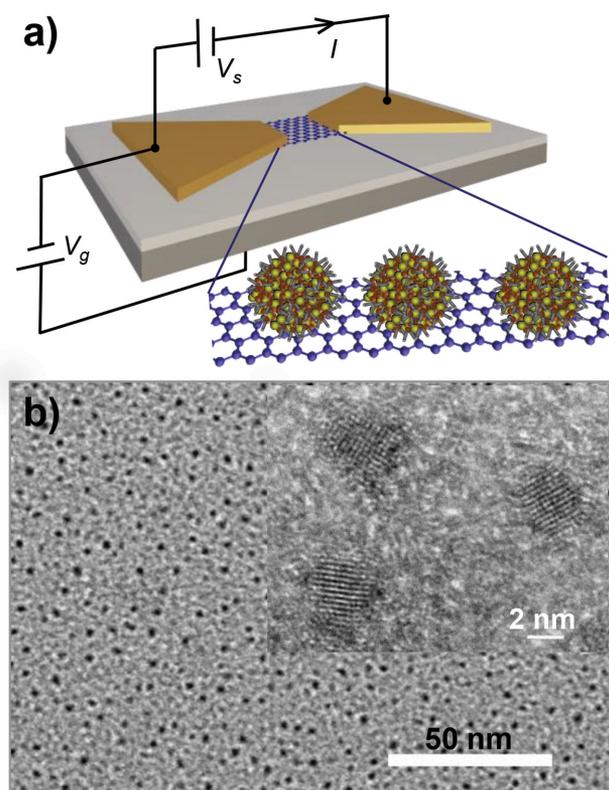
Figure 1. a) Schematic diagram of the device and circuit arrangement. b) TEM and HRTEM (inset) images of QDs (QD$_{p500}$) deposited on a graphene oxide TEM support film.

changes in its electrical properties. In dark conditions, the minimum conductance point, corresponding to a minimum concentration of carriers in the graphene layer and the Fermi energy at the Dirac point, shifts to negative gate voltage (**Figure 2**a–c). Furthermore, the conductivity of the SLG decorated with TGL/DTG capped QDs changes from p- to n-type (Figure 2c).

All three QD-decorated SLG devices are highly sensitive to light. Illumination with an unfocused laser beam ($\lambda = 514$ nm, $P \approx 10$ W cm^{-2}) leads to a photoinduced shift of the minimum in the $I(V_g)$ curve by $\Delta V_g^{\text{light}} = -3$ and -2 V toward n-type for QD$_{p2000}$ and QD$_{p500}$, respectively, and by $\Delta V_g^{\text{light}} = +8$ V toward p-type for QD$_{\text{TGL}}$, see Figure 2a–c. A measurable photoresponse

in the QD$_{p2000}$ and QD$_{p500}$ devices is detected with illumination power down to 10 W m^{-2} and at much lower powers, down to 10^{-4} W m^{-2}, for QD$_{\text{TGL}}$. These correspond to a high photoresponsivity of up to $\approx 10^9$ A W^{-1} for QD$_{\text{TGL}}$ (**Figure 3**a), which exceeds significantly the value of $\approx 10^7$ A W^{-1} measured at an excitation wavelength, $\lambda = 532$ nm, previously reported for similar size PbS QDs capped with bidentate ligands.[9] The photoresponsivity is sensitive to gate voltage and is stable over a wide range of V_g (inset of Figure 3a). Photocurrent is observed only for photon energies above the band-gap energy of the QDs and its spectrum resembles closely the QD absorption spectrum (Figure 3b). Correspondingly, the photoresponsivity of the device decreases by less than a factor of 10 for excitation wavelength increasing from the visible to the near-infrared ($\lambda \approx 1$ μm).

To explain the properties of our QD-decorated SLG devices, we first consider the positions of the energy levels of the QDs and the Dirac point of graphene, as shown schematically in **Figure 4**. We estimate the LUMO (conduction band) and HOMO (valence band) energy levels of the QDs with respect to the vacuum using the following relation based on the effective mass approximation:[10,21]

$$E_{\text{LUMO}} = E_{\text{CB}}^{\text{PbS}} + \left(E_g^{\text{QD}} - E_g^{\text{PbS}}\right)\frac{m_h^*}{m_h^* + m_e^*} \qquad (1)$$

Here, $E_{\text{CB}}^{\text{PbS}}$ and E_g^{PbS} are the electron affinity and band-gap of bulk PbS at 300 K, E_g^{QD} is an energy gap determined from the measured peak in the absorption spectrum; m_e^* and m_h^* are the electron and hole effective masses of bulk PbS.[22] This relation gives a value of $E_{\text{LUMO}} = -4.20$ eV, in good agreement with ab initio calculations for QDs of similar size.[23] For the electron affinity of graphene, we use the value $E_D^{\text{graphene}} = -4.5$ eV,[24,25] giving a LUMO level for the QDs that lies above the Dirac point of graphene, as shown schematically in Figure 4a. When the QDs come into contact with graphene, the electronic charge will redistribute itself to bring the chemical potentials in the component layers into equilibrium. Unpassivated bonds on the QD surface are known to form carrier traps with energy levels in the energy gap.[26]

The observed reduction of the hole concentration in the graphene layer is fully consistent with the transfer of electronic

Table 1. Properties of the QD layers and electrostatic model calculations.

|	QD$_{p2000}$	QD$_{p500}$	QD$_{TGL}$
Ligand	H(O⌒)$_n$O⌒H n=2000	H(O⌒)$_n$O⌒H n=500	HO⌒OH⌒SH, HO⌒SH⌒SH
Length, l [nm]	10	5	0.5
$d_{QD} + 2l$ [nm]	24.5	14.5	5.5
QD density [m^{-2}]	1.9×10^{15}	5.5×10^{15}	3.8×10^{16}
F_{QD} [V m^{-1}]	8.9×10^6	2.5×10^7	1.8×10^8
Equivalent ΔV_g [V]	2.7	7.6	53
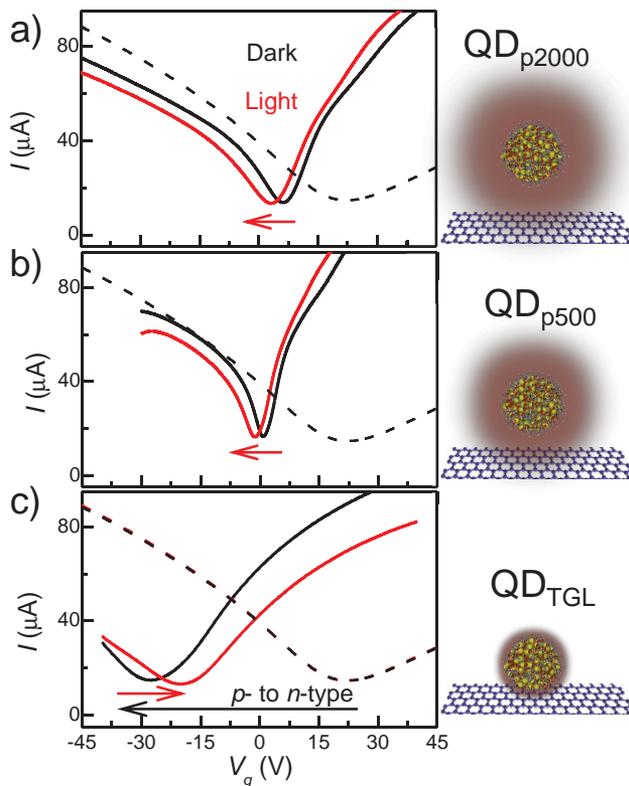
Figure 2. Current versus gate voltage characteristics, $I(V_g)$, of graphene layer before (dashed lines) and following the decoration of graphene with a) QD_{p2000}, b) QD_{p500}, and c) QD_{TGL} (black lines). $I(V_g)$ characteristics under illumination with unfocused laser light ($\lambda = 514$ nm) with $P = 10$ W m^{-2} at $V_s = 0.1$ V are shown in red. Insets show schematic representations of QDs capped with different ligands (not to scale).


Figure 3. a) Photoresponsivity of the QD_{TGL} device as a function of incident light intensity ($\lambda = 514$ nm); the dashed line is a guide to the eye. Inset: responsivity as a function of gate voltage at $V_s = 0.1$ V. b) Dependence on photon energy of the photocurrent (incident power $P \approx 10^{-11}$ W) at different gate voltages.

charge to it from the adjacent QDs. Our measurements on the three devices under dark conditions also reveal a systematic variation of the shift, ΔV_g^{dark}, with respect to the value of V_g^{dark} at the conductance minimum of pristine graphene, see Figure 4b. The measured ΔV_g^{dark} values increase with the decreasing length, l, of the capping ligands from QD_{p2000}, through QD_{p500} to QD_{TGL}, suggesting that the charge transfer is influenced by the QD capping layer. We note that our observed values of ΔV_g are comparable to those reported for similar size PbS QDs coated with bidentate ligands[9] or lipoic acid.[10]

A simple electrostatic model allows us to estimate the sheet charge density, σ_{QD}, on the quantum dot layer from the measured values of ΔV_g^{dark}. To maintain the chemical potential of the graphene layer at the Dirac point and the measured conductance at its minimum value, it is necessary to apply additional gate voltage, $\Delta V_g^{dark} \approx \sigma_{QD} t / \varepsilon_r \varepsilon_0$, following the capping of the graphene layer with the QDs; here, t and $\varepsilon_r = 3.9$ are the thickness and dielectric constant of the SiO$_2$ layer, respectively. Assuming that the QDs remain either neutral or else contain a single charge, we obtain the following value for the sheet density of dots, N, that have become charged following their deposition on the graphene layer: $N = 3.6 \times 10^{16}$ m^{-2}. Interest-

ingly, this value is close to the sheet density of a single layer of hexagonally close-packed spheres of diameter 5.5 nm (Table 1). This coincidence can be explained by noting that the accumulation of charge on the QD layer adjacent to the graphene acts to minimize the Coulomb energy of the system. The discrepancy between the measured and modeled ΔV_g^{dark} is likely due to the difference between the estimated and real thickness of dielectric layer formed by long-chain ligands resulting from the suppression of polymer chain upon drying in vacuum and/or under the weight of the QD layer.

Our electrostatic model band diagrams are shown schematically in Figure 4. Following deposition of QD_{p2000} and QD_{p500} layers and the equilibration of charge, the band diagram takes the form shown in Figure 4c. Here, the two chemical potentials are aligned, the SLG Fermi energy shifts by +50 meV, as estimated from the model in ref. [27], remaining below the QD LUMO state, and the conduction remains p-type at $V_g = 0$. Hence for devices QD_{p2000} and QD_{p500}, photoexcited electrons tend to transfer from the QDs to the graphene layer. Deposition of the QD_{TGL} results in a significantly higher level of doping of graphene, causing the SLG to become n-type at $V_g = 0$ and leading to increase of its Fermi energy by +300 meV, aligning with the LUMO energy of the QD_{TGL} device (Figure 4d). We envisage that doping-induced increase of the Fermi energy suppresses electron transfer resulting in photoexcited holes being preferentially transferred to the SLG. Our measurements of the QD_{TGL} device also demonstrate a transfer of photoexcited holes to the SLG (Figure 2).

We now consider the temporal response of the devices. **Figure 5**c shows the time-dependent photoresponse of QD_{TGL} device and reveals the presence of a slow ($\tau \approx 1$ s) and a fast ($\tau < 10^{-3}$ s) response. Similar behavior has been reported previously for
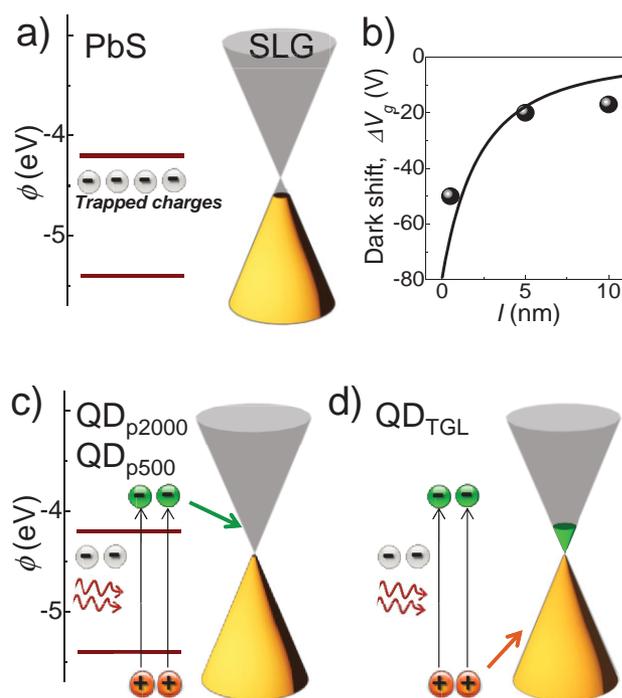
Figure 4. a) Schematic representation of the energy states before depositing the capped QDs on graphene. b) Dependence of the measured dark shift, ΔV_g, of the conductance minimum, as a function of ligand length, l. The black line is obtained from the electrostatic model discussed in the text. Alignment of the chemical potentials following QD deposition for QD_{p2000}, c) QD_{p500} and d) QD_{TGL}. Under illumination, c) photoexcited electrons or d) holes are preferentially transferred from the QDs to graphene.

other QD-decorated devices [9,10,28] and can be attributed to different mechanisms, including a slow trapping/release of charge on surface states in the QDs, charge transfer between the QDs
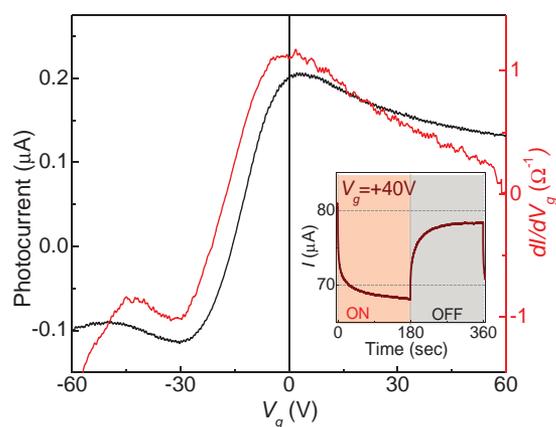

Figure 5. Comparison of photocurrent (red curve) and derivative of dark current versus gate voltage for device QD_{TGL}. Inset: temporal response at $V_g = 40V$ (lock-in frequency = 17 Hz).

and SLG, and charging/discharging of the gate capacitance by the photogenerated charge in the QDs. As shown in Figure 5, the gate voltage dependence of the photocurrent (measured using an amplifier at a lock-in frequency of 17 Hz) is qualitatively similar to that of dI/dV_g in the dark. Hence, it is likely that charging/discharging of the gate capacitance represents a dominant contribution to the temporal dynamics of this device.

Our photoconductivity measurements demonstrate that the QD layer acts as a light-sensitive gate electrode in which the photogenerated charge that remains in the QDs produces an electric field-induced change of the Fermi energy and conductance of the underlying graphene layer. For the QD_{TGL} devices, which have the highest photoresponsivity, this leads to a gate voltage shift of up to +8 V (see Figure 2c). The insulating barrier of organic ligands between the QD_{TGL} "top gate" and SLG is ≈500 times thinner than the SiO_2 barrier between the SLG and the bottom n-Si gate. Thus, a significant shift of the bottom gate voltage is induced by only a relatively small density of photogenerated charge in the QD layer (see Table 1).

In our devices, the layer of capping ligands separating the QDs and SLG retains its integrity as the QDs do not undergo any treatment following the deposition. Ligand exchange has been reported[9] to enhance the performance of devices with a QD layer. However, this process induces structural disorder in the QD films[26] and reduces the quantum yield due to oxidation of the QDs.[29] In our case, the confluent layer of capping molecules provides a uniform separation of the QDs from the SLG, thus reducing electrostatic disorder and enhancing the carrier mobility. Our $I(V_g)$ curves indicate that there is up to a fourfold increase of mobility from $\mu = 0.5$ up to 2 m² V⁻¹ s⁻¹ following QD deposition. This increase is estimated from the gradient, dI/dV_g, of $I(V_g)$[30] and is consistent with our Hall effect measurements on QD-decorated SLG devices (see Supporting Information, Figure S2). Following a 2 h thermal annealing at 200 °C which removes the capping ligands, the position of the Dirac point shifts back toward its original value and the carrier mobility decreases. This indicates that the loss of integrity of the dielectric layer leads to a nonuniform separation between the charged QD-layer and the SLG, giving rise to electrostatic disorder in the SLG sheet and hence reducing the mobility. The increased mobility of CVD graphene shortens the transit time of carriers in graphene, τ_{trans}, thus contributing to the enhancement of the photoconductive gain.

Our observation of enhanced photoresponsivity in the devices decorated with the QDs which have the shortest ligands, QD_{TGL}, indicates more efficient PbS-SLG charge transfer and thus reduced recombination of the photoexcited exciton in the PbS nanocrystals. This results in increased amount of residual positive charge in the QD layer at a given light intensity. Using a simple model, we obtain the following expression for the photoresponsivity

$$R = \frac{\alpha e}{h\nu} \frac{\tau_{QD}}{\tau_{trans}} \quad (2)$$

Here $\alpha = \alpha_i s$ is the absorbance of the PbS QDs, $\alpha_i \approx 10^5\, cm^{-1}$ is the corresponding absorption coefficient,[31] $s \approx 50\, nm$ is the QD layer thickness,[32] τ_{QD} is a lifetime of the residual photogenerated charge on the QD and $\tau_{trans} = L^2/\mu V_s = 2 \times 10^{-10}\, s$

is the electron transit time, as derived from the measured mobility of graphene. Using Equation (2) we obtain a value of $\tau_{QD} \approx 0.8\,s$. This value is in reasonable agreement with the relatively long time dynamics observed in the temporal dependence of the photocurrent for QD_{TGL} shown in the inset of Figure 5. We therefore ascribe the significantly enhanced photoresponsitivity which we report here to the three key characteristics of our devices: enhanced carrier mobility in SLG resulting in low electron transit time, high efficiency of the photo-gate arising from the long life of the photoexcited holes in the dots, and efficient charge transport at the QD–SLG interface.

In conclusion, we have shown that the characteristics of QD-decorated SLG devices are strongly affected by the properties of the QD capping layer, which acts as a dielectric barrier. The charge transfer from the QD layer and a corresponding accumulation of charge contribute to the strong photoresponse of the devices, while the presence of capping ligands affects the carrier mobility. We have demonstrated that a very high responsivity of 10^9 A W^{-1} can be achieved by selecting the length of the capping ligands and by preserving their integrity. This value is two orders of magnitude higher than previously reported for this type of device. Our results demonstrate a means of modifying the electronic properties of CVD graphene sheets and the potential of hybrid QD-graphene layers in future optoelectronic devices, particularly for high sensitivity photodetection over an extended wavelength range.

Supporting Information

Supporting Information is available from the Wiley Online Library or from the author.

Acknowledgements

[1] G. Fiori, F. Bonaccorso, G. Iannaccone, T. Palacios, D. Neumaier, A. Seabaugh, S. K. Banerjee, L. Colombo, *Nat. Nanotechnol.* **2014**, *9*, 768.

[2] Z. Sun, H. Chang, *ACS Nano* **2014**, *8*, 4133.

[3] J. Li, L. Niu, Z. Zheng, F. Yan, *Adv. Mater.* **2014**, *26*, 5239.

[4] C. O. Kim, S. Kim, D. H. Shin, S. S. Kang, J. M. Kim, C. W. Jang, S. S. Joo, J. S. Lee, J. H. Kim, S.-H. Choi, E. Hwang, *Nat. Commun.* **2014**, *5*, 3249.

[5] F. Xia, H. Wang, D. Xiao, M. Dubey, A. Ramasubramaniam, *Nat. Photonics* **2014**, *8*, 899.

[6] L. Britnell, R. M. Ribeiro, A. Eckmann, R. Jalil, B. D. Belle, A. Mishchenko, Y.-J. Kim, R. V. Gorbachev, T. Georgiou, S. V. Morozov, A. N. Grigorenko, A. K. Geim, C. Casiraghi, A. H. Castro Neto, K. S. Novoselov, *Science* **2013**, *340*, 1311.

[7] W. Zhang, C.-P. Chuu, J.-K. Huang, C.-H. Chen, M.-L. Tsai, Y.-H. Chang, C.-T. Liang, Y.-Z. Chen, Y.-L. Chueh, J.-H. He, M.-Y. Chou, L.-J. Li, *Sci. Rep.* **2014**, *4*, 3826.

[8] X. Huang, X. Qi, F. Boey, H. Zhang, *Chem. Soc. Rev.* **2012**, *41*, 666.

[9] G. Konstantatos, M. Badioli, L. Gaudreau, J. Osmond, M. Bernechea, F. P. Garcia de Arquer, F. Gatti, F. H. L. Koppens, *Nat. Nanotechnol.* **2012**, *7*, 363.

[10] D. Zhang, L. Gan, Y. Cao, Q. Wang, L. Qi, X. Guo, *Adv. Mater.* **2012**, *24*, 2715.

[11] J. Y. Kim, O. Voznyy, D. Zhitomirsky, E. H. Sargent, *Adv. Mater.* **2013**, *25*, 4986.

[12] R. Buonsanti, D. J. Milliron, *Chem. Mater.* **2013**, *25*, 1305.

[13] P. R. Brown, D. Kim, R. R. Lunt, N. Zhao, M. G. Bawendi, J. C. Grossman, V. Bulovic, *ACS Nano* **2014**, *8*, 5863.

[14] X. Li, W. Cai, J. An, S. Kim, J. Nah, D. Yang, R. Piner, A. Velamakanni, I. Jung, E. Tutuc, S. K. Banerjee, L. Colombo, R. S. Ruoff, *Science* **2009**, *324*, 1312.

[15] N. R. Wilson, A. J. Marsden, M. Saghir, C. J. Bromley, R. Schaub, G. Costantini, T. W. White, C. Partridge, A. Barinov, P. Dudin, A. M. Sanchez, J. J. Mudd, M. Walker, G. R. Bell, *Nano Res.* **2013**, *6*, 99.

[16] K. Susumu, B. C. Mei, H. Mattoussi, *Nat. Protocols* **2009**, *4*, 424.

[17] P. Flory, *Principles of Polymer Chemistry*, Cornell University Press, Ithaca, NY **1953**, ISBN 0-8014-0134-8.

[18] L. Turyanska, U. Elfurawi, M. Li, M. W. Fay, N. R. Thomas, S. Mann, J. H. Blokland, P. C. M. Christianen, A. Patanè, *Nanotechnology* **2009**, *20*, 315604.

[19] A. Das, S. Pisana, B. Chakraborty, S. Piscanec, S. K. Saha, U. V. Waghmare, K. S. Novoselov, H. R. Krishnamurthy, A. K. Geim, A. C. Ferrari, A. K. Sood, *Nat. Nanotechnol.* **2008**, *3*, 210.

[20] S. Ryu, L. Liu, S. Berciaud, Y.-J. Yu, H. Liu, P. Kim, G. W. Flynn, L. E. Brus, *Nano Lett.* **2010**, *10*, 4944.

[21] J. Jasieniak, J. Pacifico, R. Signorini, A. Chiasera, M. Ferrari, A. Martucci, P. Mulvaney, *Adv. Funct. Mater.* **2007**, *17*, 1654.

[22] The Landolt-Bornstein database, http://www.springermaterials.com/docs/index.html, (accessed: 2013).

[23] S. Z. Bisri, E. Degoli, N. Spallanzani, G. Krishnan, B. J. Kooi, C. Ghica, M. Yarema, W. Heiss, O. Pulci, S. Ossicini, M. A. Loi, *Adv. Mater.* **2014**, *26*, 5639.

[24] G. Fiori, A. Betti, S. Bruzzone, G. Iannaccone, *ACS Nano* **2012**, *6*, 2642.

[25] R. Garg, N. K. Dutta, N. R. Choudhury, *Nanomaterials* **2014**, *4*, 267.

[26] J. H. Engel, A. P. Alivisatos, *Chem. Mater.* **2014**, *26*, 153.

[27] L. Britnell, R. V. Gorbachev, R. Jalil, B. D. Belle, F. Schedin, A. Mishchenko, T. Georgiou, M. I. Katsnelson, L. Eaves, S. V. Morozov, N. M. R. Peres, J. Leist, A. K. Geim, K. S. Novoselov, L. A. Ponomarenko, *Science* **2012**, *335*, 947.

[28] Y. Q. Huang, R. J. Zhu, N. Kang, J. Du, H. Q. Xu, *Appl. Phys. Lett.* **2013**, *103*, 143119.

[29] Z. Ning, O. Voznyy, J. Pan, S. Hoogland, V. Adinolfi, J. Xu, M. Li, A. R. Kirmani, J.-P. Sun, J. Minor, K. W. Kemp, H. Dong, L. Rollny, A. Labelle, G. Carey, B. Sutherland, I. Hill, A. Amassian, H. Liu, J. Tang, O. M. Bakr, E. H. Sargent, *Nat. Mater.* **2014**, *13*, 822.

[30] S. V. Morozov, K. S. Novoselov, M. I. Katsnelson, F. Schedin, D. C. Elias, J. A. Jaszczak, A. K. Geim, *Phys. Rev. Lett.* **2008**, *100*, 016602.

[31] I. Moreels, D. Kruschke, P. Glas, J. W. Tomm, *Opt. Mater. Express* **2012**, *2*, 496.

[32] 0.1 mL of QDs at concentration 10^{17} QD L^{-1} is used for deposition on the device. For the QDs of diameter 4.5 nm this corresponds to overall QD volume of $V_{QD} \approx 10^{18}$ nm^3. Assuming the deposited drop spreads uniformly over an area of ≈ 25 mm^2, the thickness of the resulting QD layer $t \approx 50$ nm.